Differential Histopathology and Chemokine Gene Expression in Lung Tissues following Respiratory Syncytial Virus (RSV) Challenge of Formalin-Inactivated RSV- or BBG2Na-Immunized Mice

ULTAN F. POWER,* THIERRY HUSS,† VINCENT MICHAUD, HÉLÈNE PLOTNICKY-GILQUIN, JEAN-YVES BONNEFOY, AND THIEN NGOC NGUYEN

Centre d'Immunologie Pierre Fabre, 74164 Saint-Julien-en-Genevois, France

A BALB/c mouse model of enhanced pulmonary pathology following vaccination with formalin-inactivated alum-adsorbed respiratory syncytial virus (FI-RSV) and live RSV challenge was used to determine the type and kinetics of histopathologic lesions induced and chemokine gene expression profiles in lung tissues. These data were compared and contrasted with data generated following primary and/or secondary RSV infection or RSV challenge following vaccination with a promising subunit vaccine, BBG2Na. Severe peribronchiolitis and perivascularitis coupled with alveolitis and interstitial inflammation were the hallmarks of lesions in the lungs of FI-RSV-primed mice, with peak histopathology evident on days 5 and 9. In contrast, primary RSV infection resulted in no discernible lesions, while challenge of RSV-primed mice resulted in rare but mild peribronchiolitis and perivascularitis, with no evidence of alveolitis or interstitial inflammation. Importantly, mice vaccinated with a broad dose range (20 to 0.02 μg) of a clinical formulation of BBG2Na in aluminium phosphate demonstrated histopathology similar to that observed in secondary RSV infection. At the molecular level, FI-RSV priming was characterized by a rapid and strong up-regulation of eotaxin and monocyte chemotactic protein 3 (MCP-3) relative gene expression (potent lymphocyte and eosinophil chemoattractants) that was sustained through late time points, early but intermittent up-regulation of GRO/melanoma growth stimulatory activity gene and inducible protein 10 gene expression, while macrophage inflammatory protein 2 (MIP-2) and especially MCP-1 were up-regulated only at late time points. By comparison, primary RSV infection or BBG2Na priming resulted in considerably lower eotaxin and MCP-3 gene expression increases postchallenge, while expression of lymphocyte or monocyte chemoattractant chemokine genes (MIP-1β, MCP-1, and MIP-2) were of higher magnitude and kinetics at early, but not late, time points. Our combined histopathologic and chemokine gene expression data provide a basis for differentiating between aberrant FI-RSV-induced immune responses and normal responses associated with RSV infection in the mouse model. Consequently, our data suggest that BBG2Na may constitute a safe RSV subunit vaccine for use in seronegative infants.

Respiratory syncytial virus (RSV), a *Pneumovirus* of the family *Paramyxoviridae*, is a major respiratory pathogen. Infection often results in acute bronchiolitis or pneumonia in infants and young children and can result in persistently abnormal pulmonary function throughout childhood. In addition, adults become reinfected despite enhanced serum antibody responses. Consequently, development of an RSV vaccine is considered a World Health Organization priority. The occurrence of a severe pulmonary disease, characterized by the presence of abnormally numerous inflammatory cells (18), after subsequent natural infection in children given a formalin-inactivated RSV (FI-RSV) vaccine has greatly interfered in the development of a successful and safe RSV vaccine (21).

We explored a subunit approach to the development of a RSV vaccine and have described the construction and expression of a RSV (Long strain) G envelope glycoprotein fragment as part of a chimeric protein in *Escherichia coli* (20, 25). The polypeptide of amino acids 130 to 230 of the G protein (G2Na) is fused to BB, the albumin-binding domain of streptococcal protein G, producing BBG2Na. The immune responses induced by BBG2Na demonstrate a potent lung protective efficacy against RSV challenge in both mouse and cotton rat models of RSV infection (25). Importantly, this potent protective efficacy was maintained irrespective of whether BBG2Na was administered intraperitoneally (i.p.), intramuscularly (i.m.) or subcutaneously (s.c.) (15). The G2Na fragment contains at least five murine B-cell protectopes, one of which incorporates a stretch of amino acid residues that are completely conserved among all known RSV subgroup A and B human isolates (9) and all of which overlap with peptide reactivities in human RSV convalescent sera (24). Furthermore, we recently reported that immunizations with BBG2Na do not induce evidence of pulmonary inflammation upon RSV challenge, as demonstrated by the absence of aberrant and massive lung infiltration of macrophages, eosinophils, and T cells (23). In contrast, we found that in our BALB/c mouse model FI-RSV induced extensive immunopathology, characterized principally by massive lung infiltration of T lymphocytes, increased

* Corresponding author. Mailing address: Centre d'Immunologie Pierre Fabre, 5 av. Napoléon III, 74164 Saint-Julien-en-Genevois, France. Phone: (33)450.35.35.55. Fax: (33)450.35.35.90. E-mail: ultan.power@pierre-fabre.com.

† Present address: Transgène S.A., 67082 Strasbourg Cedex, France.

CD4$^+$/CD8$^+$ T-cell ratios, and extensive lung eosinophilia, coupled with large relative increases in interleukin 4 (IL-4), IL-5, IL-10, and IL-13 gene expression (23) and serum cytokine levels (12). Peak alterations in FI-RSV-immunized mice occurred between days 7 and 9 postchallenge.

One of the limitations of our previous immunopathology studies, however, is that a single dose of FI-RSV or BBG2Na was used. Work by others has shown that there is a dose-response effect of FI-RSV, with either too much or too little antigen leading to suboptimal enhanced histologic disease (45). Furthermore, Prince et al. (28) recently described pulmonary lesions in a cotton rat model associated with primary and secondary RSV infections and challenge of FI-RSV immunized animals. Interestingly, they reported that perivasculitis and peribronchiolitis were associated with all three conditions, although uniformly exacerbated in FI-RSV-primed cotton rats. However, intra-alveolar infiltration (alveolitis) and interstitial inflammation appeared to be unique to the latter animals. This work also provided us, therefore, with the basis to assess histological changes in mouse lungs as a function of priming antigen.

To address these issues, we report here an extensive histopathology study, in which BALB/c mice were immunized with several different doses of FI-RSV or BBG2Na adjuvanted with aluminum salts, followed by challenge with RSV and sacrifice at several time points postchallenge. These mice were compared for lung histologic alterations with those primed intranasally (i.n.) with live RSV or injected with phosphate-buffered saline (PBS) in adjuvant alone. The BALB/c mouse model was chosen for these studies because of ease of handling; our capacity to induce reproducible FI-RSV-related enhanced pathology that reflects, at least in part, the immunopathology reported in the deceased infant FI-RSV vaccinees; and the multitude of immunological and molecular reagents available to extensively characterize the mouse immune responses. We found that, while enhanced pathology was evident at all FI-RSV doses tested, the extent of the lesions was dose dependent. Consistent with previous reports in the cotton rat model (28), the principle pathologies evident were perivascular (perivascularitis) and peribronchiolar (peribronchiolitis) infiltrations, although mild alveolitis and interstitial inflammation were also observed. In contrast, no significant pathology was evident postchallenge in BBG2Na immunized mice, irrespective of the dose, nor in mice primed with live RSV. Likewise, mice undergoing primary infection had no discernible pathology in our model.

To extend the understanding of our BALB/c mouse model of enhanced pathology at the molecular level, we hypothesized that chemokine expression at early time points postchallenge may differ as a function of priming antigen, as these immune modulators are involved in the initiation and propagation of inflammatory responses by the recruitment of leukocytes at the site of infection or tissue injury. Chemokines are a superfamily of proinflammatory cytokines with chemotactic properties (for reviews, see references 29, 37, and 42). Chemokine synthesis is thus associated with the induction and maintenance of inflammatory events initiated by viral infections (for a review, see reference 14), even if also implicated in host defense by the installation of optimal antiviral defenses (34). The difference of immune-competent cell chemotactic responsiveness towards

particular chemokines might therefore greatly influence the outcome of immune responses. For example, the pathogenic potential and protective vaccine efficacy of live attenuated simian immunodeficiency viruses can be predicted by the analysis of cytokine-chemokine gene expression (1, 46). Indeed, a strong induction of chemokine gene expression was detected only in the lymph nodes of macaques infected with a pathogenic molecular clone and not in those infected with a nonpathogenic vaccine strain.

To date, chemokine expression in response to RSV infection has mainly been investigated in vitro, and a limited number of chemokines has been analyzed (2, 16, 17, 22, 31, 32). Infected airway epithelial cells, neutrophils, and eosinophils were shown to release chemokines with discrete target cell selectivity. These chemokines are thought to trigger and amplify, via autocrine and paracrine mechanisms, accumulation and activation of inflammatory cells in mucosal tissues. In fact, their biological activities are consistent with the recruitment of blood eosinophils, basophils, and T cells observed in the pathologic process of inflammation in RSV bronchiolitis. These findings were corroborated with nasal lavage fluids and lower respiratory secretions obtained from RSV infected children (2, 16).

Investigation of chemokine expression patterns might therefore also give important clues to the understanding of the FI-RSV-induced immunopathology and to the mechanisms of action and safety of BBG2Na. We therefore examined chemokine gene expression in the lungs of immunized and RSV-challenged mice. We particularly focused on chemokines whose known properties suggest a potential involvement in FI-RSV- or RSV-induced pathologies and chemokines that were shown to be produced by in vitro or in vivo RSV-infected cells. Based on structural similarities in their primary amino acid sequences, chemokines are classified into related gene families. In the C-X-C subfamily, chemotactic mainly for neutrophils and lymphocytes but not monocytes, we looked for the macrophage inflammatory protein 2 (MIP-2), gamma interferon inducible protein 10 (IP-10), and KC (gro [melanoma growth stimulatory activity gene]) transcripts. Members of the C-C family (acting primarily on monocytes, eosinophils, and lymphocytes) whose mRNA transcript levels were determined included regulated upon activation normal T-cell expressed and secreted protein (RANTES), macrophage inflammatory proteins-1α and -1β (MIP-1α and MIP-1β), monocyte chemotactic proteins 1 and 3 (MCP-1 and MCP-3), and eotaxin. Finally, determination of the mRNA levels of lymphotactin (Ltn) (a member of the C subfamily with strong T-cell chemoattractant effects) was also investigated. Our data indicated differential chemokine gene expression as a function of immunizing antigen and suggested an expression profile that may be characteristic of FI-RSV-induced enhanced pulmonary pathology.

MATERIALS AND METHODS

Mice. Specific-pathogen-free female BALB/c mice (age, 6 to 9 weeks) were purchased from IFFA CREDO, L'Arbresle, France. All animals were confirmed as seronegative vis-à-vis RSV before inclusion in the studies. Mice were fed mouse maintenance diet A04 (UAR, Villemoisin-sur-Orge, France) and water ad libitum. They were housed and manipulated according to national and European guidelines.

Vaccine antigen, viruses, and cells. The recombinant fusion protein BBG2Na was expressed and purified in *E. coli* as described (20, 25). Protein content was determined by the bicinchoninic acid method, and proteins were analyzed for purity and antigenicity by sodium dodecyl sulfate-polyacrylamide gel electrophoresis on 15% homogenous gels under reducing conditions and Western blotting using RSV-specific serum, respectively. RSV subgroup A (Long strain; ATCC VR-26; American Type Culture Collection, Manassas, Va.) was propagated in HEp-2 cells (ECACC 86030501; European Collection of Animal Cell Cultures, Porton Down, Salisbury, United Kingdom) as previously described (25). Viruses were harvested at 48 to 72 h by scraping cells into the medium. The suspension was centrifuged at $460 \times g$ for 15 min, and the resulting supernatant was used as virus stock. Stocks of FI-RSV used for these studies were prepared as described by Prince et al. (26), except that they were not concentrated by centrifugation. One stock of FI-RSV (stock 1) was stored at $-80°C$ until use, while the second (stock 2) was stored at 4°C. Except for the histopathology experiments, the FI-RSV stocks were used at concentrations previously determined to induced significant enhanced pulmonary immunopathology in mice.

Immunization and challenge procedures. To study histologic changes in mouse lungs following RSV challenge as a function of immunogen, groups of 15 mice received i.p. injections with 200-µl volumes on days 0, 14, and 24 with BBG2Na (20, 2, 0.2, or 0.02 µg) formulated in Adjuphos [A1(PO)$_4$ (400 µg of aluminum; Superfos BioSector a/s, Vedbaek, Denmark]; FI-RSV (stock 2, undiluted, 1/10 and 1/100) formulated in Alhydrogel [A1(OH)$_3$ (400 µg A1); Superfos BioSector a/s); or Adjuphos (400 µg of A1) alone in PBS. A final group received 10^5 50% tissue culture infectious doses (TCID$_{50}$) of RSV i.n. on day 0 and were otherwise bled, challenged, and sacrificed as for the other groups. On day 34 mice were challenged with 10^5 TCID$_{50}$ of RSV i.n. in 50 µl following anesthesia (2.5 ml per kg of body weight of a 4/1 mixture (vol/vol) with ketamine [Imalgène 500; Rhône Mérieux, Lyon, France] and xylasine [Rompun at 2%; Bayer, Puteaux, France]). Five mice from each group were sacrificed on days 2, 5, and 9 postchallenge by terminal cardiac exsanguination following anesthetizing. The lungs were fixed in situ by transtracheal inflation with Bouin fixative (Labonord, Villeneuve d'Asg, France), removed, and immersed in at least 10 volumes of Bouin following tracheal ligation, and coded.

To study chemokine gene expression in mice following immunization and RSV challenge, three independent experiments were undertaken. All mice were immunized three times on days 0, 14, and 24 by i.p. or i.m. injection of BBG2Na, FI-RSV (stock 1 diluted at 1/250 or stock 2 diluted at 1/100), or PBS in 20% (vol/vol) Alhydrogel. On day 31, mice were bled from the retro-orbital venous plexus to confirm anti-RSV seroconversion. On day 33, anesthetized mice were challenged with 10^5 TCID$_{50}$ of RSV by i.n. instillation. Just before challenge and at various time points, anesthetized mice were exsanguinated by cardiac puncture. Lungs were removed and were quick-frozen in liquid nitrogen prior to storage at $-80°C$ until RNA extraction or homogenization.

Serum antibody ELISAs. BBG2Na- and RSV-specific total immunoglobulin G titers were determined by enzyme-linked immunosorbent assay (ELISA) as previously described using horseradish peroxidase-conjugated rat anti-immunoglobulin G mouse antibodies (Southern Biotechnology, Birmingham, Ala.) (25). ELISA-determined titers were expressed as the reciprocal of the last dilution with an optical density (OD) of >0.15 and at least twofold that of the control well to which no sample was added.

Histopathologic analyses. Fixed lungs were processed for histology and analyzed by R. Loire in a blinded manner. The lungs were embedded in hot paraffin under vacuum (Hypercenter XP Shandon), thereby completing expansion of the pulmonary parenchyma. The tissue was sectioned dorso-ventrally in 4-µm-thick slices and stained with hematoxylin-eosin-safran. Histologic changes, including alveolitis, interstitial inflammation, perivascularitis, and peribronchiolitis were scored separately on a scale of 0 (normal tissue) to 4 (severe pathologic changes), according to Prince et al. (27, 28). The scores of each animal per time point per group were averaged, and the mean scores ± standard deviation (SD) were plotted as a function of time postchallenge.

Semiquantitatification of chemokine protein and gene expression in lung tissues. Eotaxin, MCP-1, and MIP-2 protein concentrations in lung tissue homogenates were determined by ELISA using appropriate Quantikine M Murine kits following the manufacturer's instructions (R&D Systems Inc., Minneapolis, Minn.). Lung homogenates were prepared by homogenizing half of each thawed lung in 500 µl of PBS containing appropriately diluted Complete protease inhibitor cocktail (Roche Diagnostics, Meylan Cedex, France), and using 0.5-mm-diameter Zirconia silica beads in a Mini beadbeater (Biospec Products) at 5,000 rpm for 20 s. The homogenates were centrifuged at $10,000 \times g$ for 5 min, and the supernatants were stored at 4°C overnight. Chemokine protein concentrations are presented as fractions of total lung homogenate protein concentrations determined by the bicinchoninic acid method (Pierce), i.e., relative chemokine concentration = [chemokine] (pg/ml)/[total protein] (mg/ml).

Chemokine transcripts were analyzed by adapting and optimizing a previously described reverse transcription (RT)-PCR ELISA method (23) for each chemokine. Lungs were weighed and disrupted in 1 ml of RNA-B (Bioprobe Systems, Montreuil-sous-Bois, France) using a Dounce homogenizer. Total RNA was extracted from the equivalent of approximately 1 mg of lung homogenate, and genomic DNA contamination of the samples was excluded by PCR analysis (23). The isolated RNA was reverse transcribed to cDNA using avian mycloblastosis virus reverse transcriptase and oligo dT$_{15}$ (Promega). The sequences of the PCR primers for MIP-2, IP-10, KC, RANTES, MIP-1α, MIP-1β, and MCP-1 were published by Su et al. (37); those of MCP-3 and eotaxin primers were published by Chensue et al. (8). Oligonucleotides specific for Ltn were determined using the Mac Vector software program (Oxford Molecular Group) and were 5′-TTGTGGAAGGTGTGGGGACTGAAGTC-3′ (sense) and 5′-GCAATGGGTTTGGGAACTGAG-3′ (antisense). They amplified a 368-bp product. The sequence of PCR amplification was a first step at 95°C for 10 min, followed by cycles of 15 s at 95°C, 30 s at 65°C (60°C for Ltn, 55°C for eotaxin and MCP-3), and 1 min at 72°C. To obtain nonsaturated PCRs, 30 cycles were applied to amplify RANTES cDNAs; 32 cycles were applied for IP-10, MCP-3, and Ltn cDNAs; 33 cycles were applied for KC, MIP-1α, and MIP-1β cDNAs; 34 cycles were applied for Eotaxin cDNAs; 35 cycles were applied for MIP-2 cDNAs; and 40 cycles were applied for MCP-1 cDNAs. β-Actin cDNAs were amplified as internal controls (23).

Digoxigenin-labeled PCR products were captured in a streptavidin-coated ELISA plate by hybridization with a 5′-biotinylated probe. Bound products were detected with peroxidase-conjugated antidigoxigenin antibodies in a standard colorimetric reaction. Probes were determined using the Mac Vector software program. Their sequences (and concentration, determined per milliliter of hybridization buffer) were the following: for MIP-2, 5′-CTGTCCCTCAACGGAAGAAC-3′ (25 µmol); for IP-10, 5′-CTCCATCACTCCCCTTTACC-3′ (25 µmol); for KC, 5′-ACGTGTTGACGCTTCCC TTG-3′ (25 µmol); for RANTES, 5′-TTGCCTACCTCTCCCTAGAG-3′ (7.5 µmol); for MIP-1α, 5′-CACC TGCATAGCTCCATCTC-3′ (25 µmol); for MIP-1β, 5′-TCTCTCTCCTCTTGCTCGTG-3′ (25 µmol); for MCP-1, 5′-GCCTGCTGTTCACAGTTGCC-3′ (25 µmol); for Ltn, 5′-AGACCTATATCATC TGGGAGGGGG-3′ (7.5 µmol). Sequences of MCP-3 and eotaxin probes were published by Chensue et al. (8), and their concentrations were 25 and 15 µmol/ml hybridization buffer, respectively. The OD at 405 nm (OD$_{405}$) was directly proportional to the level of target PCR product, which was subsequently normalized relative to the OD$_{405}$ detected for β-actin cDNAs.

Statistical analyses. Statistical analyses were done using the *t* test and the Kolmogorov-Smirnov test (for low sample numbers) of the Statigraphic software program (Manugistics, Rockville, Md.).

RESULTS

Histopathology. The influence of priming antigen and dose, compared with naive controls, on lung histopathology following RSV challenge was assessed by observing and semiquantifying four different pathologies of the lung tissues: perivasculitis, peribronchiolitis, interstitial inflammation, and alveolitis.

Primary infection with RSV (PBS groups) did not result in any appreciable pulmonary pathology in BALB/c mice (Fig. 1). Priming with RSV i.n. (RSV-in groups) followed by RSV challenge resulted in mild perivasculitis and peribronchiolitis in some animals, peaking at day 2 and progressively diminishing to undetectable pathology by day 9 post challenge. Most animals in these groups, however, demonstrated normal lungs. Neither interstitial inflammation nor alveolitis was evident in these animals. In stark contrast, immunizing mice with FI-RSV followed by challenge with RSV resulted in moderate to severe perivasculitis and peribronchiolitis, with the former tending to be more severe (Fig. 1). The lesions were characterized by extensive infiltration of lymphocytes and, to a lesser extent, large polynuclear cells. A dose effect was evident, with 1/10 and 1/100 dilutions inducing more-severe lesions than undiluted FI-RSV stock. Pathology peaks were evident on days 5 and 9,
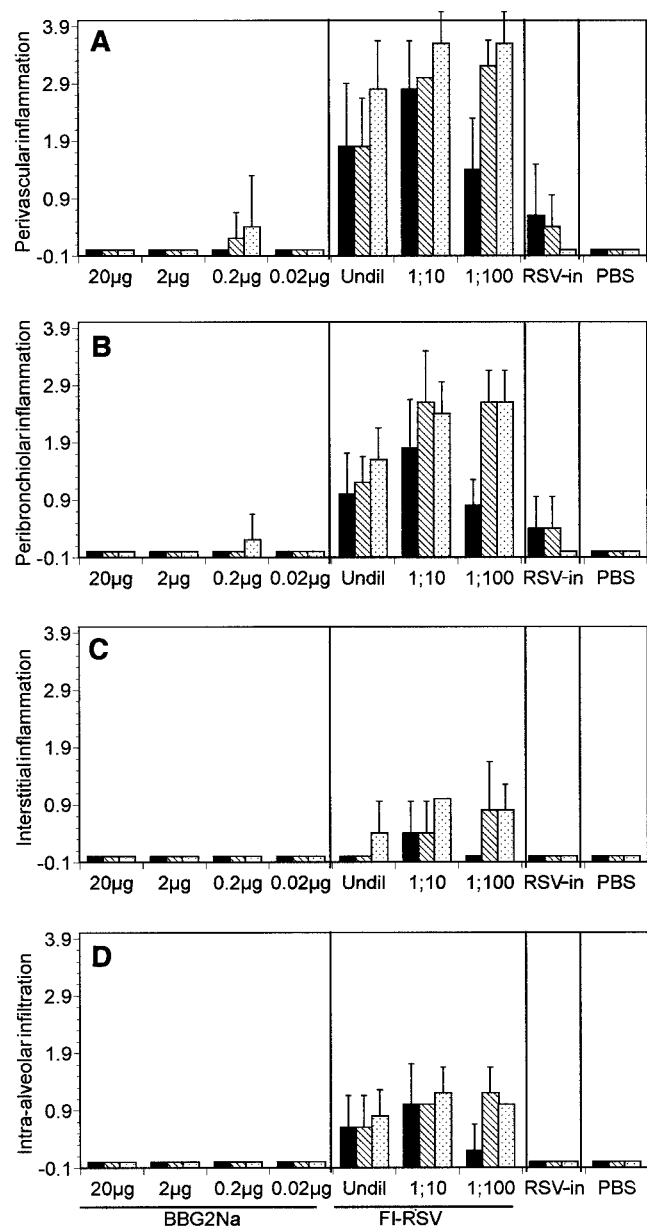
FIG. 1. Pulmonary histopathology in BALB/c mice as a function of priming antigen and time. Groups of 15 mice were immunized three times with various doses of Alhydrogel-adsorbed FI-RSV or Adjuphos-absorbed BBG2Na (as indicated below the axis) before challenge with RSV. Alternatively, groups of 15 mice were i.n. primed with RSV (RSV-in) or received PBS before RSV challenge. Mice were sacrificed on day 2 (black bars), day 5 (hatched bars), and day 9 (dotted bars) postchallenge. The lungs were inflated and fixed with Bouin, immersed in paraffin blocks, sectioned at 4 μm, and stained with hemotoxylin-eosin-safran. Histopathologic lesions, including perivascularitis (A), peribronchiolitis (B), interstitial inflammation (C), and intra-alveolar infiltration (D) were scored on the basis of normal (0) to severe (4) for each animal at each time point. Mean scores and SD (error bars) per group were plotted for each priming antigen and dose.
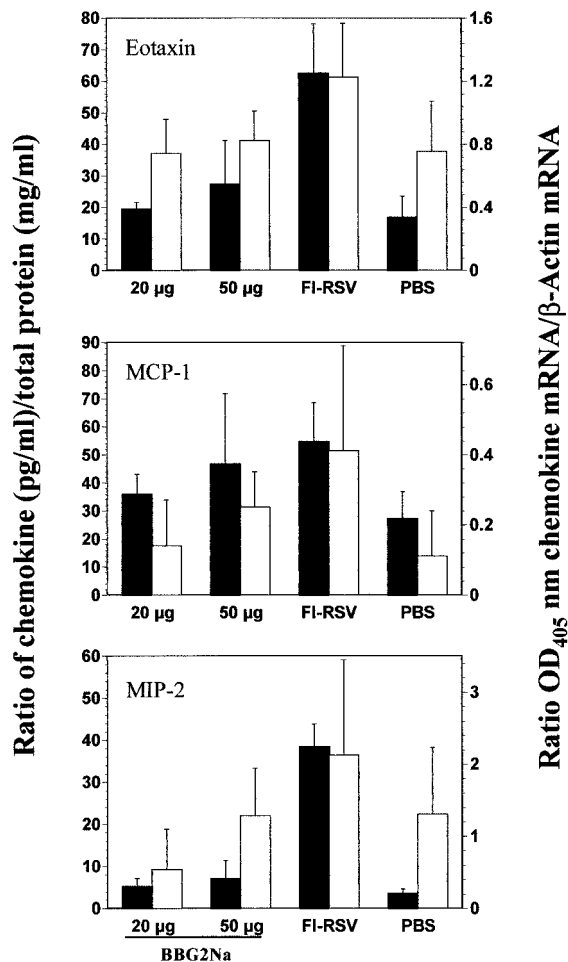

FIG. 2. Validation of semiquantitative RT-PCR assays to study chemokine gene expression profiles. Eotaxin, MCP-1, and MIP-2 protein and gene expression profiles were compared in mouse lung tissue extracts following RSV challenge, as a function of priming antigen. Groups of six mice were immunized three times i.p. with 20 or 50 μg BBG2Na, FI-RSV (stock 2 diluted at 1/100), or PBS in the presence of Alhydrogel. Mice were sacrificed 5 days after i.n. challenge with RSV. Lungs were removed and processed for either relative chemokine protein (solid bars) or gene expression (open bars) levels, as described in Materials and Methods. Chemokine protein concentrations are presented as fractions of total lung homogenate protein concentrations, i.e., relative chemokine protein concentration = [chemokine] (pg/ml)/ [total protein] (mg/ml). Chemokine gene expression data are presented as means + SD (error bars) of OD_{405} for the chemokine mRNA relative to the OD_{405} for the β-actin mRNA.

although significant infiltration was evident even at 2 days postchallenge in the group immunized with 1/10-diluted FI-RSV. Interestingly, interstitial inflammation and alveolitis were also observed in almost all mice in the FI-RSV groups,

with the latter being the more severe pathology of the two. However, these pathologies were at worst moderate and more usually mild. A dose effect and peak pathology were observed similar to those described above for perivasculitis and peribronchiolitis.

Unlike FI-RSV, no significant pulmonary pathology was evident following immunization with BBG2Na, irrespective of the dose used (Fig. 2). Indeed, of 60 animals immunized, only 1 demonstrated mild perivasculitis and peribronchiolitis, while a second had mild perivasculitis alone. In both cases, the observed pathologies were never more severe than the mild pathologies evident in the RSV-in groups. Like the RSV-in and

PBS groups, no interstitial inflammation or intra-alveolar infiltration was observed following BBG2Na immunization.

Validation of RT-PCR semiquantification of chemokine gene expression. As chemokines are intimately involved in orchestrating cell-mediated immune responses, we hypothesized that they might be implicated in the initiation and/or amplification of the abherrent pulmonary immunopathology observed in FI-RSV-immunized mice following RSV challenge. To study the temporal association of chemokines with enhanced pulmonary pathology, and in the absence of specific-protein ELISAs for each molecule, we developed semiquantitative RT-PCR assays specific for 10 different chemokine genes. We validated this approach by comparing the relative RT-PCR and protein profiles, derived using three commercial chemokine ELISA kits (eotaxin, MIP-2, and MCP-1), in lung tissues in our mouse model. As no significant histopathological differences were evident between the RSV-in and PBS groups, we limited analyses to PBS, FI-RSV, and BBG2Na groups. Groups of six mice were immunized i.p. with either 20 or 50 μg of BBG2Na, FI-RSV (stock 2), or PBS and sacrificed on day 5 postchallenge, coincident with significant histopathology in the lungs of FI-RSV immunized mice, as described above. The BBG2Na doses were chosen to bridge between previously published research doses (20 and 50 μg) (12, 23) and a dose used in a recent clinical trial (50 μg). All BBG2Na and FI-RSV-immunized mice seroconverted against RSV subgroup A antigens, as evidenced by serum ELISA titers (mean $\pm$ SD) of 4.81 $\pm$ 0.42 (20 μg), 5.05 $\pm$ 0.58 (50 μg), and 2.9 $\pm$ 0.85 log$_{10}$, respectively (not shown).

As evident in Fig. 2, both protein and RNA chemokine profiles closely resembled each other for eotaxin and MCP-1. Eotaxin was characterized by significant increases in both protein and RNA levels in the FI-RSV group relative to all other groups ($P < 0.05$). Similarly, MCP-1 protein and RNA relative concentrations were significantly higher in the FI-RSV group relative to the other groups ($P < 0.05$), except the BBG2Na, 50 μg, group. Even in this case, mean MCP-1 protein and RNA levels were higher in the FI-RSV group, with the lack of significance undoubtedly due to the large SD. MIP-2 relative protein concentrations were significantly higher in the FI-RSV group compared to all other groups ($P < 0.001$), while relative RNA concentrations were not. However, consistent with the protein ELISA data, mean MIP-2 RNA levels were highest in the FI-RSV group. These data, therefore, suggest similar antigen-specific profiles of MIP-2 gene expression and protein concentrations following RSV challenge, although the latter provides clearer differentiation between groups. Interestingly, no significant BBG2Na dose effects were evident on protein or RNA levels for any chemokine, with the exception of MIP-2 RNA levels ($P < 0.05$). In general, the combined chemokine protein and RNA data validate our semiquantitative RT-PCR assays for studying the expression kinetics of several chemokine genes in lung tissues.

Chemokine gene expression kinetics. Chemokine effects may occur early to initiate migration of cellular immune responses or later to help amplify and modulate effector functions. Therefore, we determined the kinetics of gene expression of 10 chemokines in mouse lungs following RSV challenge at early (3 to 24 h) and late time points (5 and 7 days) following RSV challenge. The later time points coincide with interme-

diate and peak inflammatory events that occur in the lungs of challenged FI-RSV-immunized animals (23). All chemokine genes examined were constitutively expressed in the lung tissues of naive nonchallenged BALB/c mice (data not shown). For the purposes of the current experiments, baseline chemokine expression levels were defined as those determined in lung tissues of PBS-injected mice just before challenge.

Whereas PBS group animals remained seronegative in these experiments, all animals of the BBG2Na and the FI-RSV (stock 1) groups efficiently seroconverted against RSV following i.m. administrations, as demonstrated by serum ELISA titers of 5.29 $\pm$ 0.33 and 3.74 $\pm$ 0.24 log$_{10}$, respectively (data not shown). Previous work in our laboratory demonstrated that sera of BBG2Na-immunized mice present relatively low neutralizing titers and that RSV was cleared from the lungs within 24 h postchallenge (25).

Prechallenge chemokine gene expression was close to baseline levels in all groups and for all chemokines (Fig. 3). At early time points following RSV challenge, FI-RSV-primed mice were characterized by progressive and large relative increases in mean eotaxin, MCP-3, and IP-10 gene expression within the first 24 h (Fig. 3). Early and intermittent upregulation of KC and MIP-2 gene expression, between 3 and 12 h, was also observed in these mice. Alternatively, no significant expression of MIP-1α, MIP-1β, or MCP-1 genes was evident, while RANTES and Ltn gene expression diminished below baseline levels during this period.

PBS control mice were characterized by progressive increases in mean MCP-3, MIP-1β, KC, IP-10, MCP-1, and MIP-2 gene expression in lung tissues at early time points (Fig. 3). In particular, MIP-1β, MCP-1 and MIP-2 were clearly upregulated compared with FI-RSV-primed mice by 12 h postchallenge. However, the levels of expression of MCP-3 and IP-10 genes were much lower than in FI-RSV primed mice. Furthermore, only small increases in eotaxin and MIP-1α were observed, while the RANTES gene expression profile resembled that of FI-RSV-primed mice. Interestingly, an initial drop below baseline levels between 3 and 12 h was followed by a significant increase in Ltn gene expression in the lungs of these mice by 24 h postchallenge.

For many of the chemokines studied, BBG2Na primed mice demonstrated lung tissue gene expression profiles at early times that closely resembled those of PBS control mice (Fig. 3). This is especially evident for eotaxin, MCP-3, KC, MCP-1, MIP-2, MIP-1α, and RANTES gene expression kinetics. While the MIP-1β expression profile paralleled that of PBS control mice during the first 12 h postchallenge, expression was intermediate between the levels observed in the PBS and FI-RSV groups by 24 h. Furthermore, the kinetics of Ltn expression up to 12 h was similar to those of both PBS control and FI-RSV-primed mice but thereafter remained below baseline expression, as in the FI-RSV-primed group. Alternatively, IP-10 gene expression kinetics in BBG2Na-primed mice during the first 24 h postchallenge were very similar to those in FI-RSV primed mice.

At later time points (days 5 and 7), while chemokine gene expression up-regulation was observed in some animals from all groups, but with the exception of RANTES, significant up-regulation above baseline was evident only in the FI-RSV group (Fig. 4). Specifically, eotaxin and MCP-3 relative expres-
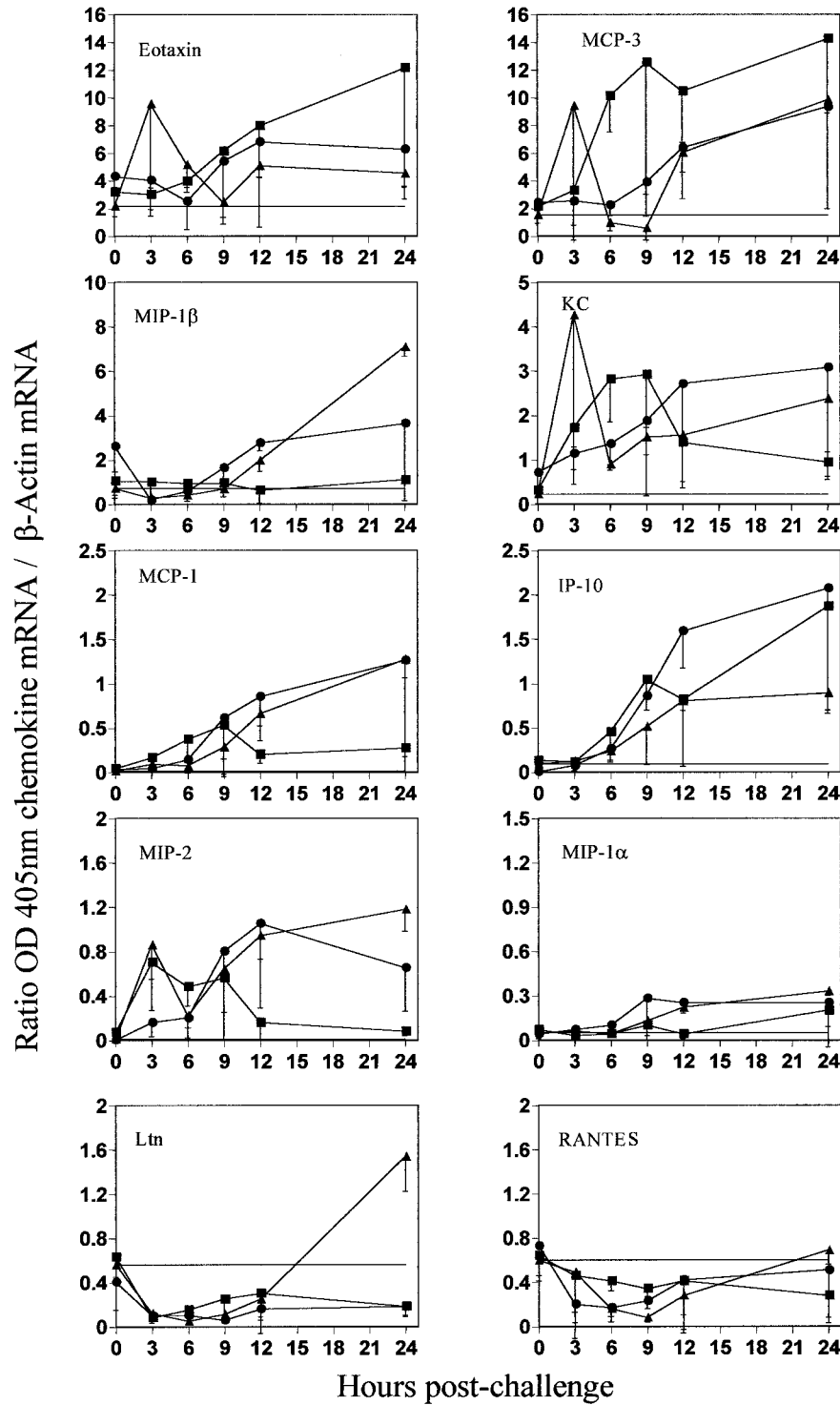
FIG. 3. Lung chemokine gene expression at early time points after RSV challenge. Groups of three to four mice were immunized three times i.m. with 50 μg of BBG2Na (●), FI-RSV (stock 1 diluted at 1/250) (■), or PBS (▲) in presence of Alhydrogel. Mice were sacrificed 3, 6, 9, 12, and 24 h after the i.n. challenge with RSV. Their lungs were removed in order to analyze chemokine gene expression by a semiquantitative RT-PCR-ELISA method. Naive unchallenged mice were used to determine the baseline level for each chemokine (horizontal line or x axis if not visible). Results shown are means ± SD (error bars) of OD_{405} for the chemokine mRNA relative to the OD_{405} for the β-actin mRNA.
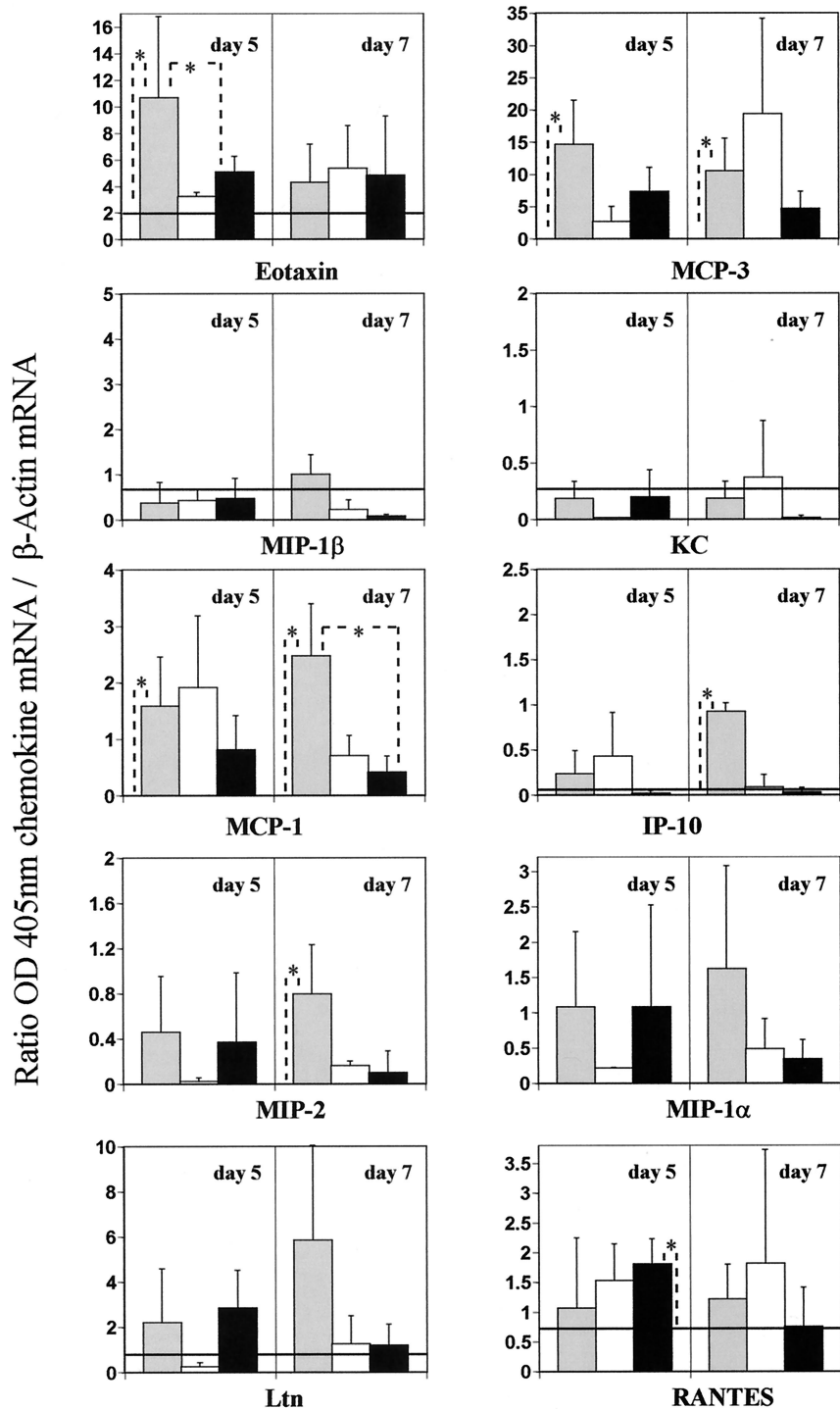
FIG. 4. Lung chemokine gene expression at later time points after RSV challenge. Groups of three to seven mice were immunized three times i.m. with FI-RSV (stock 1 diluted at 1/250) (grey bars), PBS (white bars), or 20 µg of BBG2Na (black bars), in the presence of Alhydrogel. Mice were sacrificed 5 and 7 days after the intranasal challenge with RSV. Their lungs were removed for a semiquantitative RT-PCR-ELISA analysis of chemokine gene expression. Naive unchallenged mice were used to determine the baseline level for each chemokine (horizontal lines or *x* axis if not visible). Results shown are means ± SD (error bars) of OD_{405} for the chemokine mRNA relative to the OD_{405} for the β-actin mRNA. ∗, $P < 0.05$ (calculated by the Kolmogorov-Smirnov test).

sion in this group remained high on day 5 and diminished by day 7. Interestingly, the intergroup relative expression profiles of eotaxin at late time points (Fig. 4) were consistent with those reported for the validation experiment (Fig. 2), even though absolute values and the route of immunization differed. Furthermore, IP-10 expression levels were relatively high on day 7, although not on day 5. In contrast to early time points, MCP-1 and MIP-2 genes were significantly up-regulated at later time points in the FI-RSV group, particularly on day 7. Indeed, these data were also consistent with those presented in Fig. 2, despite the difference in route of administration. As at early times, MIP-1β and KC expression remained near baseline levels at later times. While mean expression levels were above baseline, the intragroup variation in MIP-1α, Ltn, and RANTES gene expression was such that no significant increases above baseline were evident in the FI-RSV group on days 5 and 7. Conversely, in the PBS and BBG2Na groups, MIP-1β, KC, and IP-10 expression returned to baseline levels by day 5, while significant RANTES gene expression was observed only in the BBG2Na group and only on day 5.

In general, therefore, among the 10 chemokines studied, the chemokine gene expression profiles and kinetics postchallenge in the lung tissues of BBG2Na-immunized mice resembled more closely those induced following primary infection with RSV than those of mice immunized with FI-RSV. FI-RSV priming was characterized primarily by high relative expression of potent eosinophil and lymphocyte chemoattractant chemokine gene following RSV challenge (eotaxin, MCP-3, KC, and IP-10 at early time points; eotaxin, MCP-3, IP-10, MCP-1, and MIP-2 at late times). In contrast, elevated expression of mainly lymphocyte and monocyte chemoattractant chemokine genes within 24 h of challenge (MIP-1β, MCP-1, IP-10, and MIP-2) was the most striking feature of primary RSV infection or BBG2Na priming.

DISCUSSION

The failure of the FI-RSV vaccine field trials of the 1960s has enormously perturbed development of an RSV subunit vaccine for newborn infants. However, animal models of FI-RSV-associated lung-enhanced pathology have facilitated our understanding of the histology, kinetics, and mechanisms of the immunopathologic process (10, 11, 23, 26, 28, 43, 44). We extend this understanding in the current communication by describing in the mouse model the kinetics and type of histologic changes in the lung following RSV challenge as a consequence of FI-RSV priming and identifying temporally associated chemokine gene expression patterns and kinetics in lung tissues. These FI-RSV-induced histologic and chemokine gene expression changes were compared and contrasted with those resulting from primary and/or secondary RSV infection and RSV challenge of BBG2Na-primed mice.

The observation of severe histopathology in the lungs of FI-RSV-primed mice following RSV challenge is consistent with previous reports in which massive infiltration of lymphocytes and large granular cells/eosinophils into the lungs were the hallmarks of FI-RSV priming of BALB/c mice (23, 44, 45). Peak histopathology was observed between days 5 and 9, which also coincides with, and confirms, our recent observations of peak leukocyte lung infiltration (23). Furthermore, our histo-

pathology data are similar to those recently described by Prince et al. (28) for the cotton rat model of FI-RSV-induced enhanced pulmonary pathology. Indeed, enhanced pathology in the cotton rat was characterized by severe peribronchiolitis and perivascularitis coupled with aveolitis and interstitial inflammation, with the latter two pathologies being unique to FI-RSV-immunized animals. Prince et al. (28) suggested, therefore, that these lesions may provide a means of discerning unsafe vaccines. As alveolitis and interstitial inflammation were also unique to the FI-RSV-primed mice, our data suggest that these lesions may also correspond to hallmarks of enhanced pathology in the BALB/c mouse model.

However, the models diverge somewhat when lung histopathologies following primary and secondary RSV infection are compared. While invariably milder than FI-RSV priming, primary and secondary infection of cotton rats induced significant perivascularitis and peribronchiolitis. In contrast, in the mouse model, no discernible histopathology was observed after primary infection, while only mild lesions were observed following secondary infection. Our primary infection data also differ somewhat from those described by Taylor et al. (40), in which mild peribronchiolitis and perivascularitis were reported. However, both data sets suggest that the severity of perivascular and peribronchiolar lesions, coupled with the detection of alveolitis and interstitial inflammation may represent the most complete histologic indicators of unsafe vaccine-induced responses in the mouse model. In this regard, our data generated in mice primed with a clinical formulation of BBG2Na over a broad dose range are very encouraging, as very mild perivascular and peribronchiolar lesions were only rarely observed, while no alveolitis and interstitial inflammation were evident.

The differential histopathology described above confirms, as expected, that the priming antigen determines inflammatory events in the lungs following RSV challenge. We extended these data at the molecular level by profiling the expression kinetics of 10 chemokine genes in mouse lungs, with a view to further facilitating differentiation between unsafe FI-RSV-like immunopathology and potentially safe responses induced by RSV vaccines. Interestingly, while routes of immunogen administration and FI-RSV stocks differed between experiments (Fig. 2, 3, and 4), our data suggest that this did not dramatically change the relative profiles of the chemokines studied in lung tissues. This is consistent with previous work in which we demonstrated evidence of enhanced pathology postchallenge following immunization with the same FI-RSV stocks by either i.p. and i.m. routes, but not with BBG2Na (12, 23). Furthermore, doses of 20 or 50 μg BBG2Na induced comparable chemokine profiles in the lungs of BBG2Na-primed mice, thereby diminishing a potential dose effect in interpretation of our data.

Of considerable interest with regard to chemokine expression profiles, eotaxin and MCP-3 were more highly expressed at early times in the FI-RSV groups than in the other groups, suggesting that these chemokines might be good candidates for signaling molecules leading to pathology. Indeed, they are potent eosinophil and lymphocyte chemoattractants (3, 29, 35, 39, 41, 42), which comprise the principle infiltrating cells in the mouse model of FI-RSV-induced enhanced pathology (23, 43, 44). Alternatively, the relatively homeostatic kinetics of

MCP-1, MIP-1α, MIP-1β, MIP-2, Ltn, and RANTES gene expression at early time points postchallenge in this group suggest that these chemokines are not implicated in initiation of the associated pathology. The significant up-regulation exclusively in the FI-RSV groups of MCP-1 and MIP-2 expression at late time points, however, suggests that these chemokines are consequences, rather than instigators, of the cellular infiltration to the lungs. As they are potent lymphocyte chemoattractants, MCP-1 and MIP-2 might be implicated in the amplification of the immunopathologic response in the FI-RSV group once it has begun. Similarly high expression of IP-10 in FI-RSV and BBG2Na groups at early time points suggests that this chemokine is not implicated in the enhanced pathology process, despite its chemotactic properties (38), as no evidence of enhanced pathology was observed in the latter group.

The progressive increase of MCP-1, MIP-1β, and MIP-2 gene expressions at early time points in PBS control mice is consistent with previous reports of chemokine responses in RSV-infected human and murine cells in vitro (5, 17, 22, 33). It also concurs with a mainly T-cell recruitment to the lungs during primary RSV infection (23, 39). As BBG2Na-immunized mice demonstrated similar expression kinetics for these chemokines, and MIP-1β and MIP-2 are associated with preferential Th-1 type T-cell responses (30), our data might explain the lack of a recall Th-2 type T-cell response following RSV challenge of BBG2Na-primed mice (12).

The absence of a MIP-1α or RANTES expression at early time points in the PBS control group, however, contrasts with previous reports of in vitro or in vivo infections with RSV for reasons that are unclear at this time (5, 6, 7, 16, 22, 31). Similarly, in contrast to our data, infection of BALB/c mice with pneumonia virus of mice, a close relative of RSV, resulted in MIP-1 α production (13). However, no changes were observed in RANTES expression in this model, consistent with our data. Interestingly, significant Ltn expression was evident only in the PBS control group at 24 h, while it remained below baseline levels in the other groups. As Ltn is a potent T-cell chemoattractant with adjuvant properties (19) and significant T-cell lung infiltration occurs during primary RSV infection but not in BBG2Na-primed mice (23), it is possible that the differential Ltn expression may explain the presence and absence of significant T-cell infiltration in the lungs of the respective mouse groups.

Our work suggests potential key regulators of the immune responses to RSV challenge that differ according to the antigen used to prime the immune system and that confer different immunopathologic outcomes. Similar observations were made in the macaque model of siman immunodeficiency virus (SIV), in which the chemokine expression profiles were indicative of the pathogenic potential of live SIV strains (46). Briefly, *nef*-deleted SIVmac, (a live attenuated strain) was compared with wild-type SIV for chemokine expression 1 week following intravenous inoculation and correlated with subsequent disease progression. Indeed, high levels of C-C chemokines in lymph nodes correlated with disease progression following wild-type infection, while low levels were associated with nonprogression following infection with the attenuated strain. Although the animal models are very different, it may be more than an interesting coincidence that the chemokine protagonists in FI-

RSV-immunized mice at early time points postchallenge were eotaxin and MCP-3, both C-C chemokines.

The chemokine expression profiles observed in the lungs of BBG2Na-immunized animals are of particular importance. Our results indicate that T-lymphocyte and eosinophil chemoattractants were not induced at high levels upon live RSV challenge, in contrast to profiles observed in the lungs of FI-RSV-primed mice. We confirm, at the molecular level, our histopathological data presented above and previously published observations on the absence of any sign of lung inflammatory events in BBG2Na-immunized mice (23). The immunological mechanisms responsible for the innocuity of the BBG2Na vaccine candidate are not yet elucidated, but the chemokine expression profiles provide some clues for future experiments. As neither granulocytes nor increase or activation in the lymphocyte subsets was detected in the lungs of BBG2Na-immunized mice, immunosuppressive factors might also be induced at the time of vaccination or challenge.

Finally, our data demonstrate that analyzing in vivo chemokine mRNA induction in animal models following viral challenge extends our understanding at the molecular level of the immunological events associated with FI-RSV-induced lung enhanced pathology in the BALB/c mouse model. In addition to histopathology, FACScan analysis of lung-infiltrating cells, and cytokine gene expression profiles, chemokine gene expression analysis broadens the range of markers available to detect FI-RSV-like disease. Although we cannot extrapolate directly to humans, the capacity to comprehensively determine in mice whether novel RSV vaccine candidates behave like FI-RSV, or not, in terms of enhanced immunopathology will greatly increase our confidence in the innocuity of such vaccines. Indeed, it may ultimately provide a logical and scientific basis for deciding the acceptability of clinical trials with such vaccines in the principle target population for RSV vaccines, i.e., seronegative infants. In this regard, the data generated with BBG2Na thus far in the mouse model remain encouraging.

REFERENCES

1. **Ahmed, R. K. S., C. Nilsson, Y. Wang, T. Lehner, G. Biberfeld, and R. Thorstensson.** 1999. β-Chemokine production in macaques vaccinated with live attenuated virus correlates with protection against simian immunodeficiency virus (SIVsm) challenge. J. Gen. Virol. **80:**1569–1574.
2. **Alwan, W. H., W. J. Kozlowska, and P. J. Openshaw.** 1994. Distinct types of lung disease caused by functional subsets of antiviral T cells. J. Exp. Med. **179:**81–89
3. **Baggiolini, M.** 1998. Chemokines and leukocyte traffic. Nature **392:**565–568.
4. **Becker, S., W. Reed, F. W. Hendreson, and T. L. Noah.** 1997. RSV infection of human airway epithelial cells causes production of the beta-chemokine RANTES. Am. J. Physiol. **272:**L512–L520.
5. **Becker, S., and J. M. Soukup.** 1999. Airway epithelial cell-induced activation of monocytes and eosinophils in respiratory syncytial viral infection. Immunobiology **201:**88–106.
6. **Bonville, C. A., H. F. Rosenberg, and J. B. Domachowske.** 1999. Macrophage inflammatory protein-1α and RANTES are present in nasal secretions during ongoing upper respiratory tract infection. Pediatr. Allergy Immunol. **10:**39–44.
7. **Carr, M. W., S. J. Roth, E. Luther, S. S. Rose, and T. A. Springer.** 1994. Monocyte chemoattractant protein 1 acts as a T-lymphocyte chemoattrac-

tant. Proc. Natl. Acad. Sci. USA **91:**3652–3656.

8. **Chensue, S. W., K. S. Warmington, N. Lukacs, and S. L. Kunkel.** 1997. Mycobacterial and schistosomal antigen-elicited granuloma formation in IFN-gamma and IL-4 knockout mice: analysis of local and regional cytokine and chemokine networks. J. Immunol. **159:**3565–3573.

9. **Collins, P. L., K. McIntosh, and R. M. Chanock.** 1986. Respiratory syncytial virus, p. 1313–1351. *In* D. M. Knipe and P. M. Howley (ed.), Fields virology. Lippincott-Raven, Philadelphia, Pa.

10. **Connors, M., A. B. Kulkarni, C. Y. Firestone, K. L. Holmes, H. C. Morse III, A. V. Sotnikov, and B. R. Murphy.** 1992. Pulmonary histopathology induced by respiratory syncytial virus (RSV) challenge of formalin-inactivated RSV-immunized BALB/c mice is abrogated by depletion of CD4⁺ T cells. J. Virol. **66:**7444–7451.

11. **Connors, M., N. A. Giese, A. B. Kulkarni, C. Y. Firestone, H. C. Morse III, and B. R. Murphy.** 1994. Enhanced pulmonary histopathology induced by respiratory syncytial virus (RSV) challenge of formalin-inactivated RSV-immunized BALB/c mice is abrogated by depletion of interleukin-4 (IL-4) and IL-10. J. Virol. **68:**5321–5325.

12. **Corvaïa, N., P. Tournier, T. N. Nguyen, J. F. Hauew, U. F. Power, H. Binz, and C. Andreoni.** 1997. Challenge of BALB/c mice with respiratory syncytial virus does not enhance the Th2 pathway induced after immunization with a recombinant G fusion protein, BBG2Na in aluminium hydroxide. J. Infect. Dis. **176:**560–569.

13. **Domachowske, J. B., C. A. Bonville, K. D. Dyer, A. J. Easton, and H. F. Rosenberg.** 2000. Pulmonary eosinophilia and production of MIP-1α are prominent responses to infection with pneumonia virus of mice. Cell. Immunol. **200:**98–104.

14. **Friedland, J. S.** 1996. Chemokines in viral disease. Res. Virol. **147:**131–138.

15. **Goetsch, L., H. Plotnicky-Gilquin, T. Champion, A. Beck, N. Corvaia, S. Stahl, J. Bonnefoy, T. N. Nguyen, and U. F. Power.** 2000. Influence of administration dose and route on the immunogenicity and protective efficacy of BBG2Na, a recombinant respiratory syncytial virus subunit vaccine candidate. Vaccine **18:**2735–2742.

16. **Harrison, A. M., C. A. Bonville, H. F. Rosenberg, and J. B. Domachowske.** 1999. Respiratory syncytial virus-induced chemokine expression in the lower airways: eosinophils recruitment and degranulation. Am. J. Respir. Crit. Care Med. **159:**1918–1924.

17. **Jaovisidha, P., M. E. Peeples, A. A. Brees, L. R. Carpenter, and J. N. Moy.** 1999. Respiratory syncytial virus stimulates neutrophil degranulation and chemokine release. J. Immunol. **163:**2816–2820.

18. **Kim, H. W., J. G. Canchola, C. D. Brandt, G. Pyles, R. M. Chanock, K. Jensen, and R. H. Parrott.** 1969. Respiratory syncytial virus disease in infants despite prior administration of antigenic inactivated vaccine. Am. J. Epidemiol. **89:**422–434.

19. **Lillard, J. W., Jr, P. N. Boyaka, J. A. Hedrick, A. Zlotnik, and J. R. McGhee.** 1999. Lymphotactin acts as an innate mucosal adjuvant. J. Immunol **162:**1959–1965.

20. **Murby, M., E. Samuelsson, T. N. Nguyen, L. Mignard, U. F. Power, H. Binz, M. Uhlen, and S. Stahl.** 1995. Hydrophobicity engineering to increase solubility and stability of a recombinant protein from respiratory syncytial virus. Eur. J. Biochem. **230:**38–44.

21. **Murphy, B. R., S. L. Hall, A. B. Kulkarni, J. E. Crowe, Jr., P. L. Collins, M. Connors, R. A. Karron, and R. M. Chanock.** 1994. An update on approaches to the development of respiratory syncytial virus (RSV) and parainfluenza virus type 3 (PIV3) vaccines. Virus Res. **32:**13–36.

22. **Olszewska-Pazdrak, B., A. Casola, T. Saito, R. Alam, S. E. Crowe, F. Mei, P. L. Ogra, and R. P. Garofalo.** 1998. Cell-specific expression of RANTES, MCP-1, and MIP-1α by lower airway epithelial cells and eosinophils infected with respiratory syncytial virus. J. Virol. **72:**4756–4764.

23. **Plotnicky-Gilquin, H., T. Huss, J.-P. Aubry, J.-F. Haeuw, A. Beck, T. Nguyen, J.-Y. Bonnefoy, and U. F. Power.** 1999. Absence of lung immunopathology following respiratory syncytial virus (RSV) challenge in mice immunized with a recombinant RSV G protein fragment. Virology **258:**128–140.

24. **Plotnicky-Gilquin, H., L. Goetsch, T. Huss, T. Champion, A. Beck, J. F. Haeuw, T. N. Nguyen, J. Y. Bonnefoy, N. Corvaia, and U. F. Power.** 1999. Identification of multiple protective epitopes (protectopes) in the central conserved domain of a prototype human respiratory syncytial virus G protein. J. Virol. **73:**5637–5645.

25. **Power, U. F., H. Plotnicky-Gilquin, T. Huss, A. Robert, M. Trudel, S. Stahl, M. Uhlèn, T. Nguyen, and H. Binz.** 1997. Induction of protective immunity in rodents by vaccination with a prokaryotically-expressed recombinant fusion protein containing a respiratory syncytial virus G protein fragment. Virology **230:**155–166.

26. **Prince, G. A., A. B. Jenson, V. G. Hemming, B. R. Murphy, E. E. Walsh, R. L.**

Horswood, and R. M. Chanock. 1986. Enhancement of respiratory syncytial virus pulmonary pathology in cotton rats by prior intramuscular inoculation of formalin-inactivated virus. J. Virol. **57:**721–728.

27. **Prince, G. A., D. D. Porter, A. B. Jenson, R. L. Horswood, R. M. Chanock, and H. S. Ginsberg.** 1993. Pathogenesis of adenovirus type 5 pneumonia in cotton rats (*Sigmodon hispidus*). J. Virol. **67:**101–111.

28. **Prince, G. A., J. P. Prieels, M. Slaoui, and D. D. Porter.** 1999. Pulmonary lesions in primary respiratory syncytial virus infection, reinfection, and vaccine-enhanced disease in the cotton rat (Sigmodon hispidus). Lab. Investig. **79:**1385–1392.

29. **Proost, P., A. Wuyts, and J. Van Damme.** 1996. The role of chemokine inflammation. Int. J. Clin. Lab. Res. **26:**211–223.

30. **Qiu, B., K. A. Frait, F. Reich, E. Komuniecki, and S. W. Chensue.** 2001. Chemokine expression dynamics in mycobacterial (type-1) and schistosomal (type-2) antigen-elicited pulmonary granuloma formation. Am. J. Pathol. **158:**1503–1515.

31. **Saito, T., R. W. Deskin, A. Casola, H. Haeberle, B. Olszewska, P. B. Ernst, R. Alam, and P. L. Ogra.** 1997. Respiratory synytial virus induces selective production of the chemokine RANTES by upper airway epithelial cells. J. Infect. Dis. **175:**497–504.

32. **Sakai, S., H. Ochiai, H. Kawamata, T. Kogure, Y. Shimada, K. Nakajima, and K. Terasawa.** 1997. Contribution of tumor necrosis factor alpha and interleukin-1 alpha on the production of macrophage inflammatory protein-2 in response to respiratory syncytial virus infection in a murine macrophaphe cell line, RAW264.7. J. Med. Virol. **53:**145–149.

33. **Sakai, S., H. Kawamata, T. Kogure, N. Mantani, K. Terasawa, M. Umatake, and H. Ochiai.** 1999. Inhibitory effect of ferulic acid and isoferulic acid on the production of macrophage inflammatory protein-2 in response to respiratory syncytial virus infection in RAW264.7 cells. Mediators Inflamm. **8:**173–175.

34. **Salazar-Mather, T. P., J. S. Orange, and C. A. Biron.** 1998. Early murine cytomegalovirus (MCMV) infection induces liver natural killer (NK) cell inflammation and protection through macrophage inflammatory protein 1α (MIP-1α)-dependent pathways. J. Exp. Med. **187:**1–14.

35. **Schall, T. J., and K. B. Bacon.** 1994. Chemokines, leukocytes trafficking, and inflammation. Curr. Opin. Immunol. **6:**865–873.

36. **Su, Y. H., X. T. Yan, J. E. Oakes, and R. N. Lausch.** 1996. Protective antibody therapy is associated with reduced chemokine transcripts in herpes simplex virus type 1 corneal infection. J. Virol. **70:**1227–1281.

37. **Taub, D. D.** 1996. Chemokine-leukocyte interactions. The voodoo that they do so well. Cytokine Growth Factor Rev. **7:**355–376.

38. **Taub, D. D., A. R. Lloyd, K. Conlon, J. M. Wang, J. R. Ortaldo, A. Harada, K. Matsushima, D. J. Kelvin, and J. J. Oppenheim.** 1993. Recombinant human interferon-inducible protein 10 is a chemoattractant for human monocytes and T lymphocytes and promotes T cell adhesion to endothelial cells. J. Exp. Med. **177:**1809–1814.

39. **Taub, D. D., and J. J. Oppenheim.** 1994. Chemokines, inflammation and the immune system. Ther. Immunol. **1:**229–246.

40. **Taylor, G., E. J. Stott, M. Hughes, and A. P. Collins.** 1984. Respiratory syncytial virus infection in mice. Infect. Immun. **43:**649–655.

41. **Teixeira, M. M., T. J. Williams, and P. G. Hellewell.** 1997. Description of an in vivo model for the assessment of eosinophil chemoattractants in the mouse. Mem. Inst. Oswaldo Cruz **92**(Suppl. 2):211–214.

42. **Teran, L. M., and D. E. Davies.** 1996. The chemokines: their potential role in allergic inflammation. Clin. Exp. Allergy **26:**1005–1019.

43. **Vaux-Peretz, F., J. M. Chapsal, and B. Meignier.** 1992. Comparison of the ability of formalin-inactivated respiratory syncytial virus, immunopurified F, G and N proteins and cell lysate to enhance pulmonary changes in Balb/c mice. Vaccine **10:**113–118.

44. **Warris, M. E., C. Tsou, D. D. Erdman, S. R. Zaki, and L. J. Anderson.** 1996. Respiratory syncytial virus infection in BALB/c mice previously immunized with formalin-inactivated virus induces enhanced pulmonary inflammatory responses with a predominant Th2-like cytokine pattern. J. Virol. **70:**2852–2860.

45. **Warris, M. E., C. Tsou, D. D. Erdman, D. B. Day, and L. J. Anderson.** 1997. Priming with live respiratory syncytial virus (RSV) prevents the enhanced pulmonary inflammatory response seen after RSV challenge in BALB/c mice immunized with formalin-inactivated RSV. J. Virol. **71:**6935–6939.

46. **Zou, W., A. A. Lackner, M. Simon, I. Durand-Gasselin, P. Galanaud, R. C. Desrosiers, and D. Emilie.** 1997. Early cytokine and chemokine gene expression in lymph nodes of macaques infected with simian immunodeficiency virus is predictive of disease outcome and vaccine efficacy. J. Virol. **71:**1227–1236.